RSC Advances

PAPER

View Article Online
View Journal | View Issue

Cite this: RSC Adv., 2015, 5, 88655

Improvement of heat dissipation in agarose gel electrophoresis by metal oxide nanoparticles

Mohammad Zarei,[a] Elaheh K. Goharshadi,[ab] Hossein Ahmadzadeh*[a] and Sara Samiee[a]

Received 23rd September 2015
Accepted 9th October 2015

DOI: 10.1039/c5ra19678g

www.rsc.org/advances

Joule heating is a primary limitation in slab gel electrophoresis which is a gold standard method in biochemistry and biotechnology. In this paper, we introduced an innovative new class of heat transfer nanocomposites engineered by the inclusion of metal oxide nanoparticles (NPs) in a conventional separation medium (gel). The nanocomposite exhibits high thermal conductivity compared to the gel itself. The results suggest a unique correlation between the average particle size and the thermal conductivity of the metal oxide NPs with a resolution improvement in the separation, *i.e.* a reduction in Joule heating. Ceria, zirconia, tungsten oxide, and lanthania NPs were loaded into agarose gel separately and used as a separation medium for gel electrophoresis. Among the NPs, ceria with the smallest size (5.2 nm) and highest thermal conductivity (17 W m^{-1} K^{-1}) presented a better performance in reduction of Joule heating. By loading 0.3% (m/v) ceria, zirconia, and tungsten oxide NPs into the agarose gel at 25 °C, the thermal conductivity of the gel increased by 79, 78, and 78%, and resulted in a 22, 18, and 14% reduction in Joule heating (230 V), respectively. The overall separation efficiency and resolution increased for the agarose/zirconia gel as compared with the pure agarose gel. For example, the separation efficiency of the 70 and 80 (bp) peaks increased by 260 and 165%, respectively. Also, the resolution increased from 1.65 for the pure agarose gel to 6.32 for the agarose/zirconia gel.

1. Introduction

Agarose gel electrophoresis (AGE) is an important technique for the separation of biological samples.[1] However, it suffers from some physical limitations, leading to band broadening.[2] Joule heating is one of the most important factors in the band broadening phenomenon. The heat generated is directly proportional to the separation voltage, electric current, and time. Heat dissipation in slab gel electrophoresis is an important goal to enhance the separation efficiency. Capillary gel electrophoresis (CGE) has been used to resolve this problem by the efficient heat dissipation capability of the capillaries at the expense of a higher cost of the instrument and the loss of the high throughput capability of slab gel electrophoresis. Compared to slab gel electrophoresis, CGE usually needs sophisticated and expensive instruments for the analysis of biomolecules.

The addition of nanoparticles (NPs) provides unique opportunities for substantially enhancing the selectivity, efficiency, and stability of analytical techniques.[3] The application of NPs has been extensively studied in separation science.[4–9] Different types of NPs have been used successfully for separation purposes, such as carbon nanotubes,[10] fullerenes,[5] silica,[6] latex,[7] magnetic[11] and non-magnetic metal oxides,[12] and silver[13] and gold NPs.[14–17] In addition, polymer-based NPs have been used to coat silica capillaries in capillary electrophoresis.[18,19] Surprisingly, very little research has been devoted to the application of NPs in slab gel electrophoresis.[8,9]

The aims of the present study are to lower Joule heating by using a nanocomposite gel with the incorporation of metal oxide NPs, such as ceria (CeO_2), zirconia (ZrO_2), tungsten oxide (WO_3), and lanthania (La_2O_3) NPs, in agarose gel and to calculate the separation efficiency. We focused on the separation of two standard DNA samples, 100 bp and 1000 bp mixtures of highly purified DNA fragments. We investigated the influence of NPs on the porosity of agarose gel. The thermal conductivity and the Joule heating were calculated and the temperature profile of the gel was measured in order to understand the influence of the NPs on the thermal properties of the separation matrix.

2. Materials and methods

2.1. Materials

All reagents were of analytical grade. Sodium borate, hydrochloric acid, ammonia, and ethidium bromide were purchased from Merck. Zirconyl nitrate and $LaCl_3 \cdot 7H_2O$ were obtained from BDH Prolabo Chemicals. *tert*-Butyl alcohol and CTAB were purchased from Sigma-Aldrich. Sodium tungstate was purchased from Riedel. Agarose was purchased from KBC.

[a]Department of Chemistry, Ferdowsi University of Mashhad, Mashhad 91779, Iran. E-mail: h.ahmadzadeh@um.ac.ir

[b]Center of Nano Research, Ferdowsi University of Mashhad, Mashhad 91779, Iran

GeneRuler 100 bp and 1 kb DNA standards were obtained from Fermentas and were subjected to electrophoresis without further treatment.

2.2. Agarose gel electrophoresis of nucleic acids

All separations were performed on slab gels (1 × 6 × 10 cm). DNA standard samples were analyzed on 1% (m/v) agarose gel. The gels and the buffers contained 2.5 mM sodium borate buffer (pH = 8.2). Nucleic acid samples were applied to the gels in 10 pL 0.01% (m/v) bromophenol blue for DNA. Gel images were analyzed using ImageJ[20] and GelAnalyzer[21] software.

2.3. Preparation of metal oxide NPs

Ceria NPs. 2.00 g of cerium ammonium nitrate was dissolved in 20.0 mL deionized water. NaOH solution (0.18 M) was added rapidly to the solution until a white precipitate formed. The reaction vessel was then placed in a microwave (Panasonic, model: NN-C2003S, power: 1000 W) in a cycle mode of 10 s on and 5 s off (30% power). The resulting precipitate was centrifuged (10 min at 13 000 rpm) and washed with deionized water several times. Finally, the products were dried in a vacuum oven at 60 °C overnight.[22]

Zirconia NPs. ZrO_2 NPs were prepared by hydrolysis of zirconyl nitrate in aqueous alcohol solution under microwave irradiation. 50.0 mL of $ZrO(NO_3)_2$ aqueous solution (0.2 M) was mixed with 200.0 mL of *tert*-butyl alcohol. This mixture was heated to boiling point for 3 min in a microwave oven. Then, ammonia solution was added to the mixture to adjust the pH of the solution to 9.0. Subsequently, the white precipitate was centrifuged, washed with deionized water, and dried in a vacuum oven at 60 °C for 1 h. The obtained solid was calcined at 500 °C for 5 h.[23]

Tungsten oxide NPs. 30.0 mL of aqueous hydrochloric acid solution (4 M) was added to a 20 mL aqueous solution of sodium tungstate, $Na_2WO_4 \cdot 2H_2O$ (0.05 M) and stirred for 1 h at 25 °C. The solution was introduced into a Teflon tube and autoclaved for 24 h at 80 °C. The yellow precipitate was separated by centrifuging, washed several times with distilled water, and air-dried in a furnace (3 h, 250 °C).

Lanthania NPs. 0.27 g of CTAB was added to 30.0 mL of distilled water under magnetic stirring (25 °C). Then, 1.58 mmol of $LaCl_3 \cdot 7H_2O$ was added to the solution to form a homogeneous transparent solution. In order to adjust the pH of the solution to 8.5, ammonia (25%) was added dropwise to the above solution and the solution was stirred for 2 h and then transferred into a Teflon-lined stainless steel vessel and autoclaved for 24 h at 80 °C. The white solid product was centrifuged, washed with distilled water, and dried in a vacuum oven for 4 h at 80 °C. Finally, the resultant powder was calcined (4 h, 800 °C).[24]

2.4. Synthesis of nanocomposite hydrogels

In a typical synthesis, 0.20 g of agarose was dissolved in 20.0 mL of sodium borate buffer (2.5 mM) and heated to 80 °C for 10 min. An appropriate amount (0.1–0.3% (m/v)) of each type of NP was rapidly added to the agarose solution. Then, the agarose/NP solution was cooled to room temperature. A temperature probe (Misonix S-400) was used to measure the temperature in different positions of the gel (from cathode to anode).

2.5. Characterization methods

X-ray diffraction measurements were performed on a Bruker/D8 Advance diffractometer in the 2θ range from 20° to 80°, in 0.04 degree steps, using graphite monochromatic Cu Kα radiation (λ = 1.541 Å). Transmission electron microscopy (TEM) analysis of the samples was carried out on a LEO 912 AB transmission electron microscope with an electron beam accelerating voltage of 120 kV.

3. Results and discussion

3.1. Characterization

Fig. 1 shows the XRD patterns of ceria, zirconia, tungsten oxide, and lanthania NPs. In general, no additional peaks in the XRD patterns of the samples were observed which can be related to the high purity of NPs. Also, the peaks for the NPs are sharp and strong, which indicate the high crystallinity of the samples. The diffraction peaks for the ceria NPs (Fig. 1a) could be indexed to the face-centred cubic phase with the lattice parameters $a = b = c = 0.5410$ nm.

The average crystallite size of the prepared NPs was estimated using the Scherrer formula:[25]

$$D_{hkl} = \frac{k \times \lambda}{\beta_{hkl} \times \cos \theta_{hkl}} \quad (1)$$

where k is a constant (0.9), D_{hkl} is the particle size perpendicular to the normal line of the (hkl) plane, θ_{hkl} is the Bragg angle of the (hkl) peak, β_{hkl} is the full width at half maximum of the (hkl) diffraction peak, and λ is the wavelength of the X-rays. The average crystallite size of the ceria NPs was calculated as 5 nm. The diffraction peaks of the zirconia NPs were indexed to (011), (111), (002), (220), (211), (112), (220), (222), (013), and (131) reflections, which correspond to the purely monoclinic phase. The average crystallite size of the zirconia NPs was about 21 nm. The diffraction pattern of the tungsten oxide NPs (Fig. 1c) with an average crystallite size of 25 nm corresponded to the monoclinic phase. The diffraction peaks of the lanthania NPs (Fig. 1d) with an average crystallite size of 28.8 nm were indexed to (100), (002), (101), (102), (110), (103), (112), (004), (202), and (104) reflections, assigned to the hexagonal phase with lattice parameters $a = b = 0.3973$ nm and $c = 0.6129$ nm.

Fig. 2 shows TEM images with embedded particle size distributions of ceria, zirconia, tungsten oxide, and lanthania NPs. According to these images, the NPs display uniform morphology with an average size of 5.2, 26, 31.5, and 51.2 nm for the ceria, zirconia, tungsten oxide, and lanthania NPs, respectively.

3.2. Joule heating

In order to study the Joule heating effect, an Ohm plot was constructed by applying different voltages across the separation medium and monitoring the generated currents. Fig. 3 shows *I*–

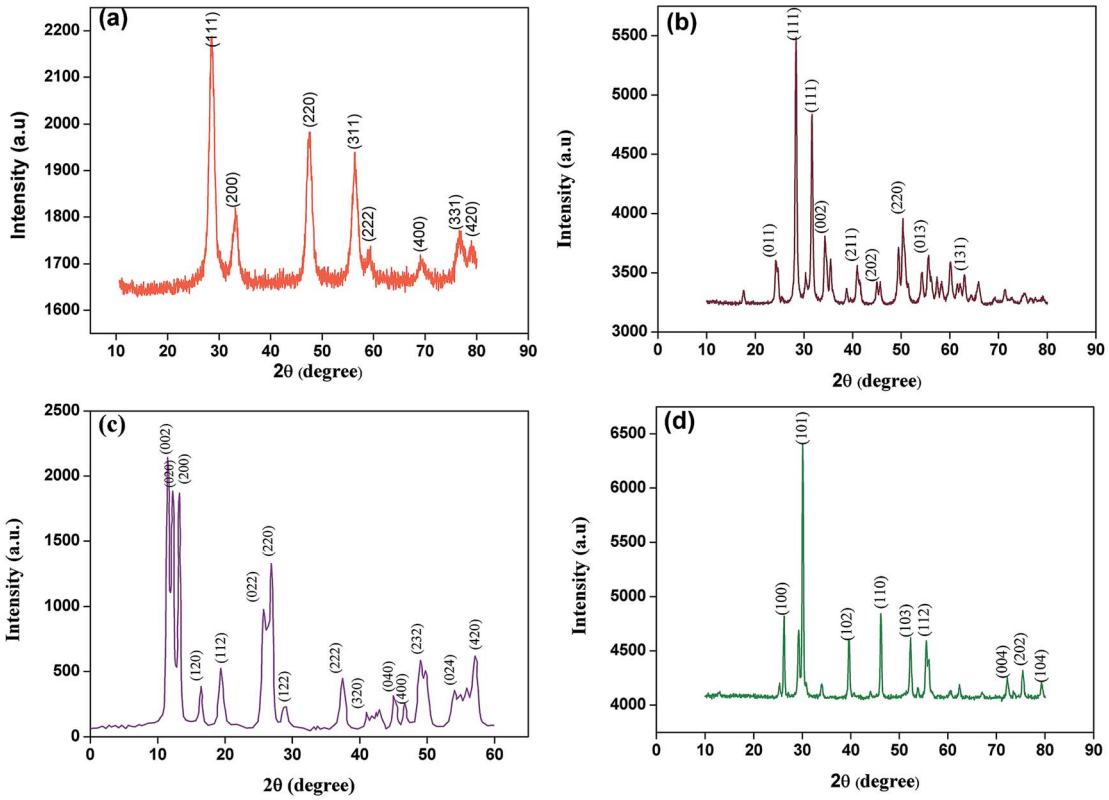

Fig. 1 XRD patterns of (a) ceria, (b) zirconia, (c) tungsten oxide, and (d) lanthania NPs.

V measurements (Ohm plot) for the agarose gel and the agarose/NP modified gels. The threshold voltage (U_t) above which the current begins to abruptly increase is the maximum separation voltage that should be applied in order to have the shortest separation time. The values of U_t in the pure agarose and the agarose/ceria, agarose/zirconia, agarose/tungsten oxide, and agarose/lanthania gels were estimated to be 170, 200, 190, 180, and 175 V, respectively. At high voltages, the produced heat in the NP embedded gels is less than that of the pure agarose gel (Fig. 3a–d). The heat generated is directly proportional to the separation voltage, *U*, electric current, *I*, and time, *t*:

$$q = UIt \quad (2)$$

Fig. 3e–h show the calculated Joule heating for the pure agarose gel and the NP embedded gels at different applied voltages. As this figure shows, by addition of the NPs to the agarose gels, the amount of Joule heating decreased. For example, at 150 V, the values of the generated heat were 16.31, 15.39, 16.17, 16.20, 16.45 kJ for the agarose, ceria/agarose, zirconia/agarose, tungsten oxide/agarose, and lanthania/agarose gels, respectively. A significant decrease in Joule heating is seen at higher applied voltages. For example, at 220 V, the values of produced heat were 18.46, 16.42, 16.75, 16.93, and 16.85 kJ in the agarose, ceria/agarose, zirconia/agarose, tungsten oxide/agarose, and lanthania/agarose gels, respectively. In the ceria/agarose gel, the produced heat reduces by 6 and 12% at 150 V and 200 V, respectively.

By increasing the percentage of NP loading, the magnitude of the Joule heating decreases further. By loading 0.3% m/v of NPs, at the applied voltages, the values of Joule heating decreased by 12, 10, 9, and 8% for the agarose/ceria, agarose/zirconia, agarose/tungsten oxide, and agarose/lanthania gels, respectively, compared to that of the pure agarose gels. The order of decrease in Joule heating has good correlation with the average particle size and the thermal conductivity of the NPs. As Table 1 shows, there is a correlation between the average particle size and the thermal conductivity of the metal oxide NPs with the reduction in Joule heating. The ceria NPs, with the smallest size and highest thermal conductivity among the NPs, reduced the Joule heating by 12% when 0.3% m/v was included in the gel. Even at a higher voltage of 230 V, by loading 0.3% m/v ceria NPs into the agarose gel at 25 °C, the thermal conductivity increased by 79%, which resulted in a 22% reduction in Joule heating and an increase in the separation efficiency. Generally, Joule heating increases with applied voltage, but in the NP modified gels, the NPs act as heat sinks and reduce the generated heat. The thermal conductivity of the metal oxide NPs increases significantly with temperature, as well as with the volume fraction of NPs.[26] This leads to a reduction of the Joule heating by the agarose/metal oxide NP gel at high voltages.

The temperature difference between the center line and the inside line of the separation medium can be calculated using the Knox equation:[27]

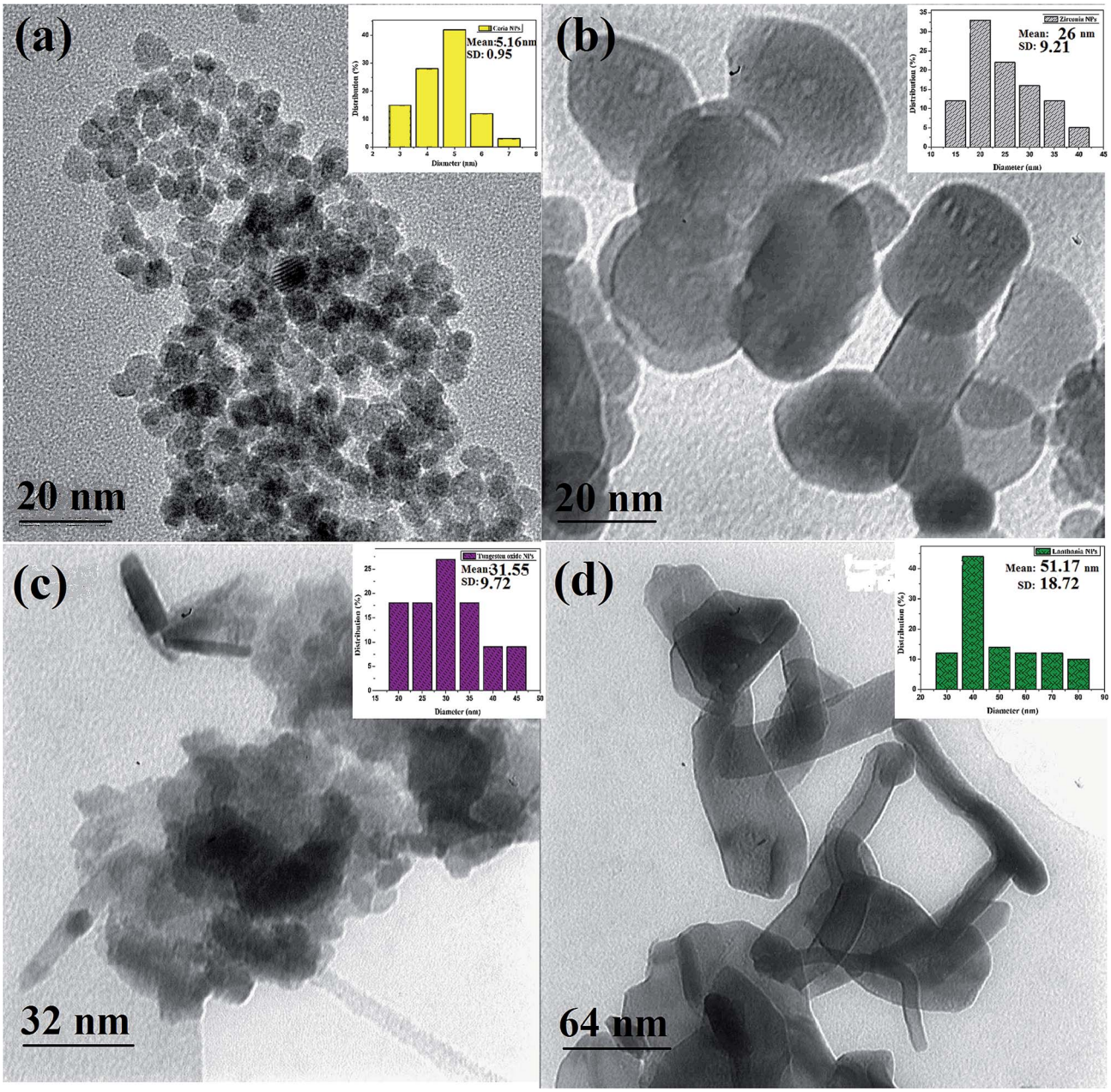

Fig. 2 TEM images and particle size distributions of prepared (a) ceria, (b) zirconia, (c) tungsten oxide, and (d) lanthania NPs.

$$\Delta T = \frac{Qr^2}{4\kappa} \tag{3}$$

where r is the radius of the separation medium, κ is the thermal conductivity, and Q is the heat produced per unit volume and time:

$$Q = \frac{UI}{whl} \tag{4}$$

where w, h, and l are the dimensions of the gel. As eqn (3) shows, there is an inverse relationship between the temperature difference and the thermal conductivity of the medium. Hence, thermal conductivity plays a vital role in the improvement of separation. The thermal conductivity of the NPs is higher than that of pure agarose gel (0.56 W m^{-1} K^{-1}).[28] Of course, choosing appropriate NPs is very important. For example, carbon nanotubes (CNTs) were included in separation gels[29,30] to improve the resolution of serum DNAs.

The main criterion is to choose NPs with high thermal conductivities and low electrical conductivities. The reason is simple: we do not wish the NPs to move and/or cause non-uniformities in the electric field, *i.e.* NPs with low electrical conductivities. At the same time, we wish the NPs to act as heat sinks to effectively dissipate heat and lower Joule heating, *i.e.* NPs with high thermal conductivities. Based on this criterion, ceria, zirconia, tungsten oxide, and lanthania NPs were chosen (Table 1).

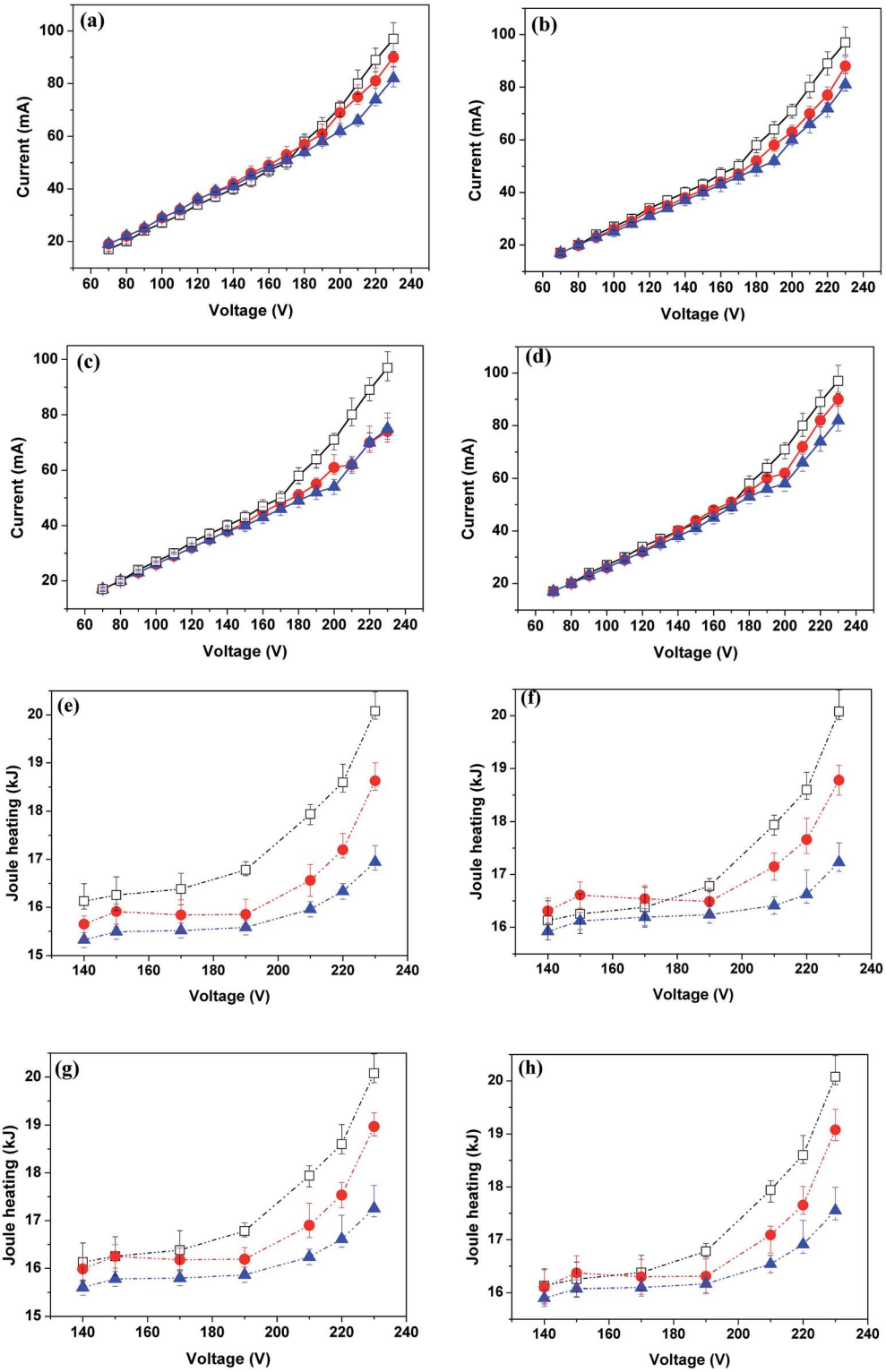

Fig. 3 Current *vs.* voltage curve for (a) agarose/ceria, (b) agarose/zirconia, (c) agarose/tungsten oxide and (d) agarose/lanthania, and the magnitudes of Joule heating *versus* applied voltage for (e) agarose/ceria, (f) agarose/zirconia lanthania, (g) agarose/tungsten oxide and (h) agarose/lanthania (□ pure agarose, ● = 0.1, ▲ = 0.3% m/v).

Table 1 Correlation between average particle size and thermal conductivity of NPs with the decrease in the magnitude of Joule heating

NPs	Average particle size[a] (nm)	Thermal conductivity of the bulk (W m^{-1} K^{-1})	Electrical conductivity of the bulk (S m^{-1})	Joule heating reduction (%)
CeO_2	5.2	17 (ref. 31)	0.044 (ref. 32)	12
ZrO_2	26.0	4.2 (ref. 33)	0.86 (ref. 34)	10
WO_3	31.5	1.6 (ref. 35)	NR[b]	9
La_2O_3	51.2	NR	10^{-5} (ref. 36)	8

[a] Calculated using TEM image. [b] Not reported.

There is an important disadvantage of using CNTs in the separation medium. CNTs have high thermal conductivity (3500 W m^{-1} K^{-1})[37] and high electrical conductivity (10^6 to 10^7 S m^{-1}).[38] CNTs move when a separation voltage is applied. That causes the depletion of CNTs on one side of the gel and accumulation on the other side. If a voltage is applied for a long time, the CNTs keep moving and might egress from the other side of the gel. The Joule heating would be lower on the side where the CNTs have migrated to, and higher on the depleted side. In this work, we chose metal oxide NPs since they have high thermal conductivity but low electrical conductivity. Hence, metal oxide NPs increase the thermal conductivity of the separation medium, without generation of a concentration gradient across the gel.

The temperature difference between the center and the edges of the gels measured using a temperature probe and calculated using the Knox equation (eqn (3)) is shown in Fig. 4. The temperature gradient in the agarose/metal oxide NPs is smaller than that of pure agarose due to the higher thermal conductivity of the NPs (Fig. 4). At 200 V, the temperature gradient across the agarose/ceria, agarose/zirconia, agarose/tungsten oxide, and agarose/lanthania gels were 0.20, 0.35, 0.60, and 1.00 °C, respectively, when the loading amount of NPs was 0.1% m/v, while its value was 2.5 °C in pure agarose gel. For a loading amount of 0.3% m/v, the temperature gradient across the agarose/ceria, agarose/zirconia, agarose/tungsten oxide, and agarose/lanthania gels was 0.17, 0.28, 0.41, and 0.77 °C, respectively. By increasing the percentage of NP loading from 0.1 to 0.3% m/v, the temperature gradient in the gel reduced further. This is related to the higher values of thermal conductivity of the gel/NPs than that of the pure agarose gel.

There are no theoretical formulae to predict the thermal conductivity of suspensions of NPs, so-called nanofluids, satisfactorily.[39] The Maxwell model,[40] a traditional model for thermal conductivity, has been proposed for solid–liquid mixtures:

$$\lambda_c = \frac{\lambda_f + 2\lambda_m + 2\phi(\lambda_f - \lambda_m)}{\lambda_f + 2\lambda_m - \phi(\lambda_f - \lambda_m)} \quad (5)$$

where λ_f and λ_m are the thermal conductivity of the nanocomposite (agarose/NP gel), the filler material (NPs), and the polymer matrix (agarose), respectively. The Maxwell model underestimates the thermal conductivity of the suspensions of NPs. This is because the model does not include the effects of particle size, particle size distribution, and temperature.[41]

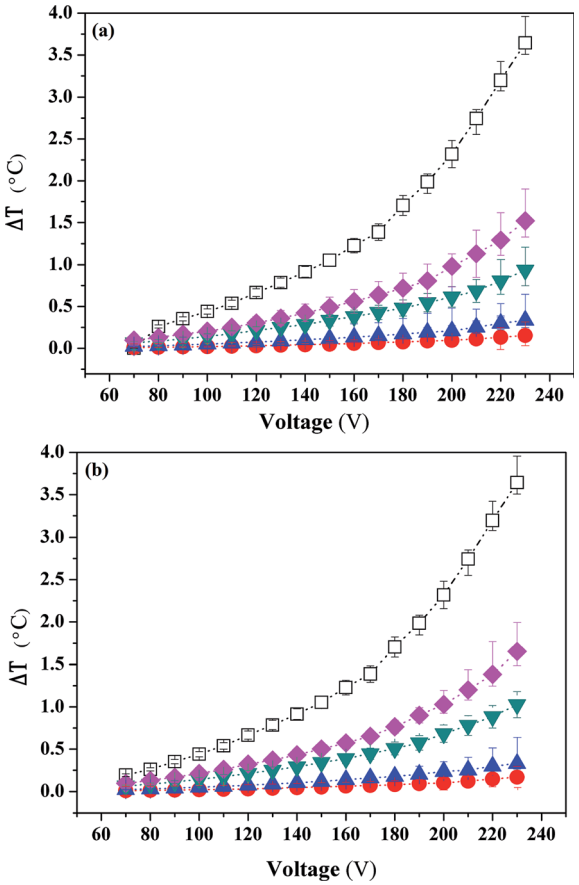

Fig. 4 Temperature difference between the center and the edges of gels at (a) 0.1% (m/v) and (b) 0.3% (m/v) (□ agarose, ● agarose/ceria, ▲ agarose/zirconia, ▼ agarose/tungsten oxide, and ◆ agarose/lanthania gels).

The thermal conductivity of agarose/ceria, agarose/zirconia, and agarose/tungsten oxide was calculated according to the Maxwell model as 1.0010, 1.0003, and 1.0061, respectively, for 0.3% (m/v) of the NPs. This is equivalent to an enhancement in thermal conductivity of 79% for agarose/ceria, 78% for agarose/zirconia, and 78% for agarose/tungsten oxide gels compared with that of the agarose gel. Hence, the NPs act as heat sinks to lower the produced heat. After careful analysis with respect to the Joule heating and thermal conductivity

measurements, the agarose/ceria and agarose/zirconia nanocomposite gels were chosen as separation media for the separation of DNA samples.

3.3. Separation of standard DNA samples by the NP modified gels

The separation panels and electropherograms of standard DNA samples (a mixture of 10 highly purified DNA fragments (100

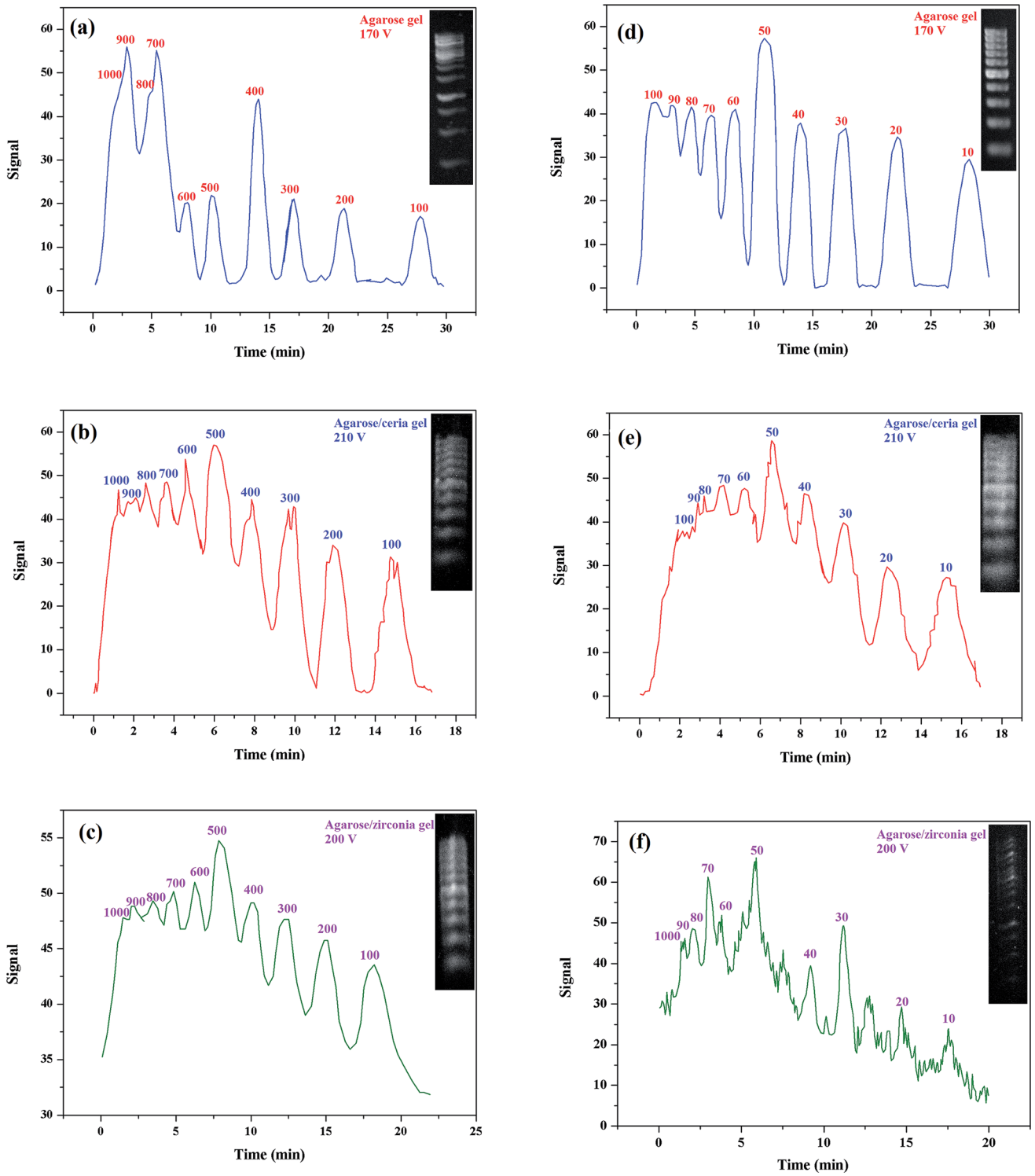

Fig. 5 The electropherograms of standard DNA sample (1 kb) on (a) pure agarose, (b) agarose/ceria and (c) agarose/zirconia, 0.3% m/v (numbers: number of base-pairs). The electropherograms of the DNA sample (100 bp) on (d) pure agarose, (e) agarose/ceria and (f) agarose/zirconia, 0.3% m/v (numbers: number of base-pairs).

bp: 10–100 bp and 1 kb: 100–1000 bp)) on agarose gel and the agarose gel/NPs are shown in Fig. 5. The separations were performed at different voltages (170, 210, and 200 V for agarose, agarose/ceria, and agarose/zirconia, respectively) chosen based on the threshold voltage for the initiation of Joule heating for agarose and agarose/NPs. Also, we compared the performance of the agarose/NPs with that of the pure gel for separation at high voltages. For the separation of the 1 kb DNA sample (Fig. 5a–c), the number of separated DNA fragments in the range of 700–1000 bp increased for agarose/ceria and agarose/zirconia compared to those of the pure agarose gel. Also, the separation time decreased in the agarose gel/NPs compared to that in the pure agarose gel because of the higher applied voltages. In the separation of the 100 bp DNA sample, the number of separated DNA fragments increased in agarose/ceria compared to that in the pure agarose gel (Fig. 5d–f).

The efficiency of the electrophoresis can be evaluated by the number of theoretical plates, N:[2]

$$N = 5.54\left(\frac{t}{w_{1/2}}\right)^2 \quad (6)$$

where t and $w_{1/2}$ stand for the migration time of the DNA fragments and the temporal peak widths at half the peak heights. The numbers of theoretical plates for the peaks 10–100 and 100–1000 for agarose, agarose/ceria, and agarose/zirconia gels are given in Table 2. The values of N increased in the agarose/zirconia gel compared to those of the agarose gel. The number of theoretical plates, N, is related to the applied voltage, U, by the following equation:[42]

$$N = \frac{zFU}{2\theta RT} \quad (7)$$

where z is the effective charge, F is the Faraday constant or the charge per mole of protons, T is temperature, R is the gas constant, and θ is the dispersion coefficient. In electrophoresis, the efficiency (N) increases with increasing voltage, as far as Joule heating allows. By incorporation of metal oxide NPs into the agarose gel, the Joule heating threshold voltage expands. This maximizes the separation efficiency and lowers the separation time.

The resolution between two peaks in the electropherogram can be calculated as:[2]

$$R_s = \frac{2(t_2 - t_1)}{w_1 + w_2} \quad (8)$$

where t_1 and t_2 are the migration times for components 1 and 2, respectively. w_1 and w_2 stand for the temporal peak widths of components 1 and 2, respectively. The appropriate resolution between components requires a combination of good selectivity and good separation efficiency ($R_s \sim N^{1/2} \sim U^{1/2}$).[43,44] The resolution between peaks was also measured. In general, the resolution increased in the agarose/zirconia gel compared to that of the agarose gel. For example, the resolution between peaks 70 and 80 (bp) increased from 1.65 for the pure agarose gel to 6.32 in the agarose/zirconia gel.

Close examination of the bands shows broad peaks for the agarose gel, whereas these broad peaks split into partially resolved peaks in the agarose/zirconia gel. This shows an enhancement in resolution when the metal oxide NPs are embedded in the agarose gel. For separation of 1 kb and 100 bp DNA fragments using agarose/zirconia gel electrophoresis, the resolution for all adjacent pairs was calculated. The results are tabulated in Table 3 and shown in Fig. 5. The separation parameters in agarose gel/zirconia and the number of separated DNA fragments significantly increased as compared to those of

Table 2 Calculated theoretical plate number of standard DNAs

	N		
Peak (bp)	Agarose gel	Ceria NPs (0.3% m/v)	Zirconia NPs (0.3% m/v)
100	354.56	101.75	176.32
200	610.78	132.65	345.36
300	400.26	124.32	246.32
400	173.73	1418.24	110.65
500	138.50	110.78	121.32
600	311.60	632.12	187.32
700	16.78	1418.81	26.32
800	—	1246.50	45.29
900	2.82	554.00	72.32
1000	—	640.12	69.31
10	694.93	265.12	2650.97
20	608.00	285.63	4989.56
30	384.56	177.32	3462.50
40	126.70	101.32	2681.36
50	122.65	234.06	3512.36
60	77.90	138.62	2216.21
70	54.10	354.56	482.59
80	43.43	635.32	384.70
90	73.12	452.31	670.34
100	46.32	532.15	571.25

Table 3 Measured resolutions of adjacent bands for standard DNAs

	R_s		
Peak (bp)	Agarose gel	Ceria NPs (0.3% m/v)	Zirconia NPs (0.3% m/v)
100–200	2.54	1.57	1.09
200–300	2.00	1.11	1.62
300–400	2.12	1.20	1.33
400–500	1.33	1.60	1.25
500–600	1.66	0.66	0.57
600–700	0.5	1.32	0.65
700–800	—	4.12	0.55
800–900	—	2.32	1.06
900–1000	—	4.65	1.12
10–20	2.58	1.55	3.33
20–30	2.10	1.50	3.56
30–40	2.15	1.62	3.00
40–50	2.32	1.55	4.12
50–60	1.71	1.12	4.28
60–70	1.62	1.09	5.12
70–80	1.65	2.59	6.32
80–90	1.81	2.01	2.31
90–100	0.65	2.25	1.23

the pure gel. The number of separated DNA fragments for separation at 210 V increased in agarose gel/ceria (0.3% m/v) compared to that of the pure gel. There is a significant decrease in the analysis time at higher voltages with the NP modified gel. For example, the separation time of DNA 100 (bp) by agarose, agarose/ceria, and agarose/zirconia is 30, 17, and 22 min, and for DNA 1 (kb) it is 30, 17, and 20 min, respectively. Also, the sharpness of the peaks increased in agarose gel/ceria. The number of peaks for the separation of long-stranded DNA fragments (100 bp: 70–100 bp, 1000 bp: 700–1000 bp) increased in both agarose/ceria and agarose/zirconia gels compared to those of the agarose gel.

The effective separation of long-stranded DNA fragments is important in comprehensive genomic analysis of DNA samples and is usually performed by pulsed field gel electrophoresis.[45] Unfortunately, pulsed field gel electrophoresis is slow and separation times are in the range of several hours to several days. Although capillary electrophoresis (CE) with entangled polymer[46] solutions has been used for the separation of DNA molecules of different sizes,[47–49] CE is not efficient for separation of long-stranded DNA due to the requirement of sophisticated and expensive instruments. Ultradilute polymer solutions,[50,51] pulsed-field CE,[52–54] entropy trap arrays,[55,56] asymmetric obstacle arrays,[57] and a DNA prism[58] have been developed to overcome the problem of time delays in CE.

Huang *et al.*[59] separated long double-stranded DNA (dsDNA) molecules using nanoparticle-filled capillary electrophoresis. They used gold nanoparticles (GNPs) modified with poly(-ethylene oxide) (PEO) to form gold nanoparticle/polymer composites (GNPPs). GNPPs are heavy and electrically neutral: thus, they slow down DNA molecule migration in electrophoresis. Polymer solutions such as PEO and GNPPs provide greater efficiency and shorter migration times for separation of long dsDNA. Polymer chains could attach to the surfaces of NPs through their hydrophobic parts, which leaves their hydrophilic groups available to interact with the polar dispersion media.

NPs can be wrapped by long single- and double-stranded DNA (ssDNA and dsDNA). ssDNA and dsDNA have different affinities toward NPs.[60] The essential difference in adsorption behavior between ssDNA and dsDNA may be attributed to their different electrostatic properties. Also, ssDNA has a flexible structure and uncoils in solution under the influence of an applied voltage. In contrast, dsDNA has a stable and rigid structure.[61] For example, long ssDNA can wrap around CNTs.[62,63] Hence, it is plausible to say that a large ssDNA fragment may adsorb onto NPs and may be trapped by NPs.

Polymer chains are adsorbed on the surface of metal oxide NPs to form an NP/polymer composite. The composite is heavy and electrically neutral, hence it slows the migration of DNA molecules. Long DNA fragments have a greater probability to interact with more than one NP, depending on the DNA size and conformation. The drag force is stronger for long DNA fragments as compared to short ones. As a result, the mobility of long DNA is smaller than that of a short one. Fig. 5 shows that for the agarose/ceria gel, the resolution and efficiency of DNAs with higher molecular weights (700–1000 bp) are greater as compared with lower molecular weight DNA (100–600 bp), which could be explained by the interaction of long stranded DNAs with the NPs' surfaces.

Incorporation of NPs into the separation medium could change the physicochemical behavior and thermal conductivity of the separation medium.[8]

3.4. Influence of the NP concentration

In order to understand the relationship between the NP concentration and the degree of improvement in the separation parameters, three different concentrations of NPs (0.1, 0.3, and 0.5% m/v) were incorporated into agarose gel. The optimum separation efficiency was obtained for 0.3% m/v NPs. However, when the concentration of the NPs is higher than 0.3% m/v, no significant improvement in separation parameters was achieved. An excess NP concentration will cause interference with the UV light produced by the gel documentation system, which increases the background of images, and lowers the S/N ratio of the separation profiles.

3.5. Influence of NPs on gel porosity

In order to understand the influence of NP incorporation on the porosity of the agarose gel, the porosity was calculated by measuring the density of dry and wetted gels. The overall gel porosity was calculated using the following formula:[64]

$$\text{Porosity}\% = \frac{\text{dry density} - \text{wetted density}}{\text{density of water}} \times 100 \qquad (9)$$

The wetted density is the ratio of the weight to volume of a gel which was saturated with a wetting liquid for 24 h at room temperature. Table 4 shows that the porosity in water increases with the amount of NP filler. For example, in a gel containing 0.1 and 0.3% m/v ceria NPs, the porosity increased by 2 and 3% with increasing filler content. The porosity of the gel was increased by increasing the amount of NPs. In general, the sharpness and resolution of all defined bands increased in the NP modified gels because the NPs alter both the chemical composition and thermal conductivity of the polymer matrix.

By introducing NPs into the matrix, the pore size distribution of the matrix changes with respect to the pure gel. The inclusion of NPs has been shown to cause nucleation, which reduces the pore size of the polymer matrix.[65] Also, as the size of the NPs decreases, the pore density increases compared to that of the gel.

Table 4 Porosity variations in NP embedded gels for different NP concentrations

	Porosity enhancement	
Matrix	0.1% m/v	0.3% m/v
Agarose/ceria	2	3
Agarose/tungsten oxide	1	2
Agarose/zirconia	2	4

4. Conclusions

Metal oxide NPs were embedded into an agarose gel to increase the separation efficiency by reducing Joule heating and lowering band broadening. The influence of the NPs on Joule heating was successfully evaluated. A reduction in Joule heating was observed by dispersing the NPs in agarose gel. The results showed a unique correlation between the average particle size and the thermal conductivity of the metal oxide NPs with a reduction in the amount of generated heat. Among the metal oxide NPs studied, ceria with the smallest size (5.2 nm) and highest thermal conductivity (17 W m^{-1} K^{-1}) presented a better performance in lowering the Joule heating.

The optimum separation efficiency was obtained for 0.3% m/v NPs. For example, by loading 0.3% m/v ceria NPs in agarose gel at 25 °C, the thermal conductivity increased by 79%, which resulted in a 22% reduction in Joule heating and an increase in the separation efficiency. Finally, this paper presents the potential to improve the separation efficiency and resolution of other biomolecules using slab gel electrophoresis.

Acknowledgements

The authors acknowledge the ATF committee and Ferdowsi University of Mashhad for supporting this project (3/23032). The authors also thank Dr Razieh Jalal and Dr Ahmad Reza Bahrami for their generous donation of DNA standards.

Notes and references

1 B. D. Hames, *Gel Electrophoresis of Proteins: A Practical Approach*, Oxford University Press, 1998.
2 R. Kuhn and S. Hoffstetter-Kuhn, *Capillary Electrophoresis: Principles and Practice*, Springer-verlag, Berlin, 1993.
3 C. R. Martin and D. T. Mitchell, *Anal. Chem.*, 1998, **70**, 322A–327A.
4 L. Yang, E. Guihen, J. D. Holmes, M. Loughran, G. P. O'Sulliva and J. D. Glennon, *Anal. Chem.*, 2005, **77**, 1840–1846.
5 M. R. Ivanov and J. H. Amanda, *Analyst*, 2011, **136**, 54–63.
6 L. Tang, X. Wang, B. Guo, M. Ma, B. Chen, S. Zhan and S. Yao, *RSC Adv.*, 2013, **3**, 15875–15886.
7 D. Xiao, C. Zhang, D. Yuan, J. He, J. Wu and H. He, *RSC Adv.*, 2014, **4**, 64843–64854.
8 M. Zarei, H. Ahmadzadeh and E. K. Goharshadi, *Analyst*, 2015, **140**, 4434–4444.
9 M. Zarei, H. Ahmadzadeh, E. K. Goharshadi and A. Farzaneh, *Anal. Chim. Acta*, 2015, **887**, 245–252.
10 H. Luo, Z. Shi, N. Li, Z. Gu and Q. Zhuang, *Anal. Chem.*, 2001, **73**, 915–920.
11 A. Manbohi, S. H. Ahmadi and V. Jabbari, *RSC Adv.*, 2015, **5**, 57930–57936.
12 A. Kolmakov and M. Moskovits, *Annu. Rev. Mater. Res.*, 2004, **34**, 151–180.
13 A. D. McFarland and R. P. van Duyne, *Nano Lett.*, 2003, **3**, 1057–1062.
14 E. Guihen and J. D. Glennon, *Anal. Lett.*, 2003, **36**, 3309–3336.
15 T. B. L. Kist and M. Mandaji, *Electrophoresis*, 2004, **25**, 3492–3497.
16 V. Sharma, K. Park and M. Srinivasarao, *Mater. Sci. Eng.*, 2009, **65**, 1–38.
17 C.-S. Wu, F.-K. Liu and F.-H. Ko, *Anal. Bioanal. Chem.*, 2011, **399**, 103–118.
18 G. Kleindienst, C. G. Huber, D. T. Gjerde, L. Yengoyan and G. K. Bonn, *Electrophoresis*, 1998, **19**, 262–269.
19 C. G. Huber, A. Premstaller and G. Kleindienst, *J. Chromatogr. A*, 1999, **849**, 175–189.
20 M. D. Abràmoff, P. J. Magalhães and S. J. Ram, *Biophotonics Int.*, 2004, **11**, 36–43.
21 I. Lazar and I. Lazar, *Gel Analyzer 2010a: Freeware 1D Gel Electrophoresis Image Analysis Software*, 2012.
22 E. K. Goharshadi, S. Samiee and P. Nancarrow, *J. Colloid Interface Sci.*, 2011, **356**, 473–480.
23 E. K. Goharshadi and M. Hadadian, *Ceram. Int.*, 2012, **38**, 1771–1777.
24 E. K. Goharshadi, T. Mahvelati and M. Yazdanbakhsh, *J. Iran. Chem. Soc.*, 2015, 1–8.
25 P. Scherrer, *Nachr. Ges. Wiss. Goettingen, Geschaeftliche Mitt.*, 1918, **2**, 96–100.
26 C. H. Li and G. Peterson, *J. Appl. Phys.*, 2006, **99**, 084314.
27 J. Knox and I. Grant, *Chromatographia*, 1987, **24**, 135–143.
28 M. Zhang, Z. Che, J. Chen, H. Zhao, L. Yang, Z. Zhong and J. Lu, *J. Chem. Eng. Data*, 2010, **56**, 859–864.
29 G. Huang, Y. Zhang, J. Ouyang, W. R. Baeyens and J. R. Delanghe, *Anal. Chim. Acta*, 2006, **557**, 137–145.
30 Y. Guo, L. Huang, W. R. Baeyens, J. R. Delanghe, D. He and J. Ouyang, *Nano Lett.*, 2009, **9**, 1320–1324.
31 M. Khafizov, I. W. Park, A. Chernatynskiy, L. He, J. Lin, J. J. Moore, D. Swank, T. Lillo, S. R. Phillpot and A. El-Azab, *J. Am. Ceram. Soc.*, 2014, **97**, 562–569.
32 J. L. Rupp and L. J. Gauckler, *Solid State Ionics*, 2006, **177**, 2513–2518.
33 J. F. Bisson, D. Fournier, M. Poulain, O. Lavigne and R. Mévrel, *J. Am. Ceram. Soc.*, 2000, **83**, 1993–1998.
34 G. Cao, *J. Appl. Electrochem.*, 1994, **24**, 1222–1227.
35 J. Liqiang, Q. Yichun, W. Baiqi, L. Shudan, J. Baojiang, Y. Libin, F. Wei, F. Honggang and S. Jiazhong, *Sol. Energy Mater. Sol. Cells*, 2006, **90**, 1773–1787.
36 V. Lazarev, V. Krasov and I. Shaplygin, *Electrical Conductivity of Oxide Systems and Film Structures*, Nauka, Moscow, 1979.
37 E. Pop, D. Mann, Q. Wang, K. Goodson and H. Dai, *Nano Lett.*, 2006, **6**, 96–100.
38 Q. Li, Y. Li, X. Zhang, S. B. Chikkannanavar, Y. Zhao, A. M. Dangelewicz, L. Zheng, S. K. Doorn, Q. Jia and D. E. Peterson, *Adv. Mater.*, 2007, **19**, 3358–3363.
39 E. Goharshadi, H. Ahmadzadeh, S. Samiee and M. Hadadian, *Phys. Chem. Res.*, 2009, **1**, 1–33.
40 R. Kochetov, A. Korobko, T. Andritsch, P. Morshuis, S. Picken and J. Smit, *J. Phys. D: Appl. Phys.*, 2011, **44**, 395401.
41 M. Abareshi, E. K. Goharshadi, S. M. Zebarjad, H. K. Fadafan and A. Youssefi, *J. Magn. Magn. Mater.*, 2010, **322**, 3895–3901.

42 J. Giddings, *Unified Separation Science*, John Wiley and Sons, New York, 1991, ch. 8, p. 166.
43 Y. Ito and J. Cazes, *Encyclopedia of Chromatography*, Taylor & Francis, 2001.
44 J. C. Reijenga, in *Encyclopedia of Chromatography*, Taylor & Francis, 2nd edn, 2005, p. 121.
45 D. C. Schwartz and C. R. Cantor, *Cell*, 1984, **37**, 67–75.
46 K. D. Cole and C. M. Tellez, *Biotechnol. Prog.*, 2002, **18**, 82–87.
47 Y. Kim and E. S. Yeung, *J. Chromatogr. A*, 1997, **781**, 315–325.
48 F. Han, B. H. Huynh, Y. Ma and B. Lin, *Anal. Chem.*, 1999, **71**, 2385–2389.
49 H. Zhou, A. W. Miller, Z. Sosic, B. Buchholz, A. E. Barron, L. Kotler and B. L. Karger, *Anal. Chem.*, 2000, **72**, 1045–1052.
50 A. E. Barron, D. S. Soane and H. W. Blanch, *J. Chromatogr. A*, 1993, **652**, 3–16.
51 B. Braun, H. W. Blanch and J. M. Prausnitz, *Electrophoresis*, 1997, **18**, 1994–1997.
52 W. Volkmuth and R. Austin, *Nature*, 1992, **358**, 600–602.
53 Y. Kim and M. D. Morris, *Anal. Chem.*, 1995, **67**, 784–786.
54 H. Oana, M. Ueda and K. Yoshikawa, *Electrophoresis*, 1997, **18**, 1912–1915.
55 J. Han and H. Craighead, *Science*, 2000, **288**, 1026–1029.
56 J. Han and H. G. Craighead, *Anal. Chem.*, 2002, **74**, 394–401.
57 C.-F. Chou, O. Bakajin, S. W. Turner, T. A. Duke, S. S. Chan, E. C. Cox, H. G. Craighead and R. H. Austin, *Proc. Natl. Acad. Sci. U. S. A.*, 1999, **96**, 13762–13765.
58 L. R. Huang, J. O. Tegenfeldt, J. J. Kraeft, J. C. Sturm, R. H. Austin and E. C. Cox, *Nat. Biotechnol.*, 2002, **20**, 1048–1051.
59 M.-F. Huang, Y.-C. Kuo, C.-C. Huang and H.-T. Chang, *Anal. Chem.*, 2004, **76**, 192–196.
60 H. Deng, X. Zhang, A. Kumar, G. Zou, X. Zhang and X.-J. Liang, *Chem. Commun.*, 2012, **49**, 51–53.
61 H. Li and L. Rothberg, *Proc. Natl. Acad. Sci. U. S. A.*, 2004, **101**, 14036–14039.
62 W. Zhao, Y. Gao, M. A. Brook and Y. Li, *Chem. Commun.*, 2006, 3582–3584.
63 F. Zhao, H. Cheng, Y. Hu, L. Song, Z. Zhang, L. Jiang and L. Qu, *Sci. rep.*, 2014, **4**, 1–7.
64 K. de Sitter, C. Dotremont, I. Genné and L. Stoops, *J. Membr. Sci.*, 2014, **471**, 168–178.
65 K. Goren, L. Chen, L. S. Schadler and R. Ozisik, *J. Supercrit. Fluids*, 2010, **51**, 420–427.